INTERNATIONAL JOURNAL OF QUANTUM CHEMISTRY, VOL. 42, 1101–1114 (1992)

Theoretical Study of the Hydrogen Chemisorption on a ZnO Surface

H. NAKATSUJI AND Y. FUKUNISHI

Division of Synthetic Chemistry, Faculty of Engineering, Kyoto University, Kyoto 606, Japan

Abstract

Reactions of a hydrogen molecule with a ZnO surface are studied by an ab initio method. For simulating the ZnO (10 $\bar{1}$ 0) surface, one ZnO molecule both with and without a Madelung potential is used. Since the electrostatic potential due to the ionic layer decreases exponentially, the effect of the layers deeper than the second one can be neglected. The Madelung potential is, therefore, expressed by the 32 point charges of ±0.5 situated on the first and second layers. Several low-lying states of ZnO and the ZnO + H_2 system have been calculated by the symmetry-adapted cluster (SAC) and SAC–CI methods. It is found that the $^1\Sigma^+$ state of ZnO is the ground state and catalytic active and the other states are inactive. ZnO ($^1\Sigma^+$) reacts with H_2 and dissociatively adsorbs it with making Zn—H and O—H bonds. This occurs both with and without the Madelung potential. Without the Madelung potential, the heat of reaction is 81.3 kcal/mol and the reaction barrier is 14.0 kcal/mol. With the Madelung potential, the heat of reaction decreases to 73.5 kcal/mol and the barrier decreases to 11.5 kcal/mol. The mechanism of this reaction is the electron donation from the $2p\pi$ orbital of O to the antibonding σ_u MO of H_2 and the back-donation from the bonding σ_g MO of H_2 to the LUMO of ZnO. In the intermediate stage of the reaction, the dipole of ZnO works to increase the overlap of the active MOS to make the reaction easier. Throughout the reaction, the in-plane $2p\pi$ orbital of O and the HOMO of ZnO are inactive and work to keep the ZnO bond stable during the catalytic process.

1. Introduction

Zinc oxide is an *n*-type semiconductor and has a catalytic activity for hydrogenations of olefins. It is a wultzite-type crystal and has many stable surfaces. It dissociatively adsorbs the hydrogen molecule, and the existence of some adsorbed hydrogen species is known. Particularly, type I hydrogen shows a rapid and reversible adsorption and is responsible for the O—H and Zn—H IR peaks observed at 1710 and 3510 cm^{-1}, respectively. This species is the principal source of hydrogen for the hydrogenation of ethylene [1]. Type II hydrogen, on the other hand, contributes little to the hydrogenation of ethylene and does not give Zn—H and O—H bands, but it promotes the rate of the catalytic reaction. Type III hydrogen exists at temperatures near 78 K. This is molecularly adsorbed on the same site as the type I species [2].

On the theoretical side, some relevant papers have been published in recent years. Anderson and Nichols studied the adsorption of hydrogen on the ZnO

 CCC 0020-7608/92/051101-14$04.00

(10 $\bar{1}$ 0) surface by a semiempirical molecular orbital method. They found that heterolytic adsorption of H_2 allows the formation of strong O—H and Zn—H bonds, but homolytic adsorption results in two weak Zn—H bonds [3]. Bauschlicher and Langhoff studied low-lying electronic states of ZnO and ZnS. They calculated the spectroscopic constants and the dipole moments for the $^{1,3}\Sigma^+$ and $^{1,3}\Pi$ states of ZnO and ZnS by the configuration–interaction and coupled-pair methods [4]. Dolg et al. studied early transition-metal monoxides by the SD–CI method [5]. Gropen et al. calculated the diatomic oxides of Sc, Ti, Cr, Ni, and Zn in order to test the reliability of the pseudopotential methods [6]. Witko and Koutecky studied the potential curves of $ZnO + C_2H_4$ and $(ZnO + C_2H_4)^+$ systems using pseudopotential-MRD–CI and all-electron MRD–CI methods [7]. An attractive interaction has been found for several excited states of the $ZnO + C_2H_4$ system.

We study here hydrogen chemisorption on the ZnO (10 $\bar{1}$ 0) surface. We calculate the reaction path for the H_2 chemisorption on ZnO surrounded by a Madelung potential represented by an array of a limited number of point charges. We examine the effect of the Madelung potential on the low-lying states of ZnO and on the activity of ZnO for the dissociative adsorption of H_2. We show the reorganization of the electron density along the reaction process. The conclusion of the present study is given in the last section.

2. Computational Method

The Gaussian basis for the Zn atom is the (3*s*2*p*5*d*)/[2*s*2*p*2*d*] set and the Ar core is replaced by the effective core potential [8]. For the O atom, we use the Huzinaga–Dunning [4*s*2*p*] basis [9] plus diffuse *sp* functions (exponent 0.059) and polarization *d* functions (exponent 0.30). For the H atom, we use the Huzinaga–Dunning (4*s*)/[2*s*] set plus *p*-type functions that are the first derivatives of the [2*s*] set. Then, the Hellmann–Feynman theorem is satisfied for the forces acting on the hydrogen nuclei [10]. Calculating the Hellmann–Feynman forces acting on the H atoms, we examine the path of approach of H_2 onto ZnO for which the distance is fixed at 1.95 Å, an experimental value for the crystal. We calculate the potential energy curves of the ground and excited states by the symmetry-adapted cluster (SAC)/SAC–CI method [11, 12]. We use 37 active orbitals, nine orbitals being occupied and 28 orbitals being unoccupied. The linked operators in the SAC/SAC–CI calculation are selected by using the thresholds λg and λe of 1×10^{-5} and 2×10^{-5} au [13], respectively. The wave function consists of 3000–5000 linked operators that are symmetry-adapted in each spin symmetry. The Hartree–Fock calculations are performed with the use of the program GAMESS [14], and the SAC/SAC–CI calculations, by the program SAC85 [15].

For simulating the ZnO (10 $\bar{1}$ 0) surface, one ZnO molecule embedded in a Madelung potential is used. The Madelung potential is expressed by the 32 point charges of ± 0.5 situated on the first and second layers, which are illustrated in Figure 1. The electrostatic potential due to the ionic layer decreases exponentially, and the one due to the charges that are situated in the *z* axis decreases

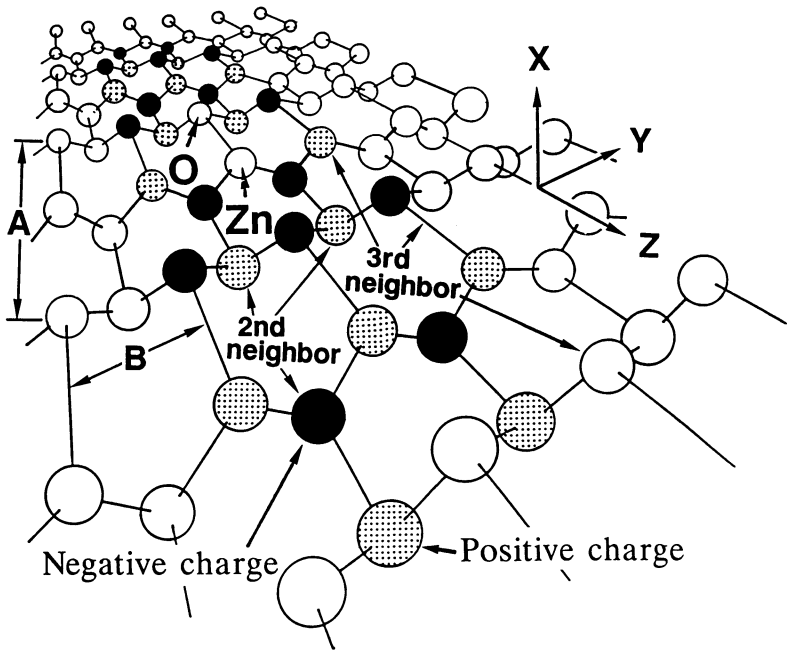

Figure 1. ZnO (10 $\bar{1}$ 0) surface and the array of 32 point charges used in this calculation.

more rapidly, as shown in the Appendix. Therefore, the electrostatic potential made by the 32 point charges located around the ZnO molecule reach to 92% of the one due to 6886 point charges. The Madelung potential is proportional to the ionic charge, q, in $Zn^{+q}O^{-q}$. There are several ways of estimating this quantity, but the results are widely spread, namely, $q \sim 1$ [16], $q \sim 0.8$ [17], and $q \sim 0.4$ [18]. The Mulliken's atomic charge of ZnO calculated by the Hartree–Fock method is ± 0.6. However, the smaller value should be used for q because of the electron spacial distribution. We then choose a point charge of ± 0.5.

3. Results and Discussion

A. ZnO

We calculate the potential curves of the low-lying states of ZnO by the SAC/SAC–CI method. The results are shown in Figure 2. The ground state is $^1\Sigma^+$ for the Zn—O distance shorter than 1.98 Å, but at a larger distance, the $^3\Pi$ state becomes the ground state. The equilibrium bond length of the $^1\Sigma^+$ state is 1.76 Å, which is shorter than the distance in the crystal, 1.95 Å. The bonding orbital is made of the 4s orbital of Zn and the $2p\sigma$ orbital of O. The binding energy is 20 kcal/mol and the dipole moment at the point of equilibrium is 5.82 Debye. These results are in good agreement with the results of the previous theo-

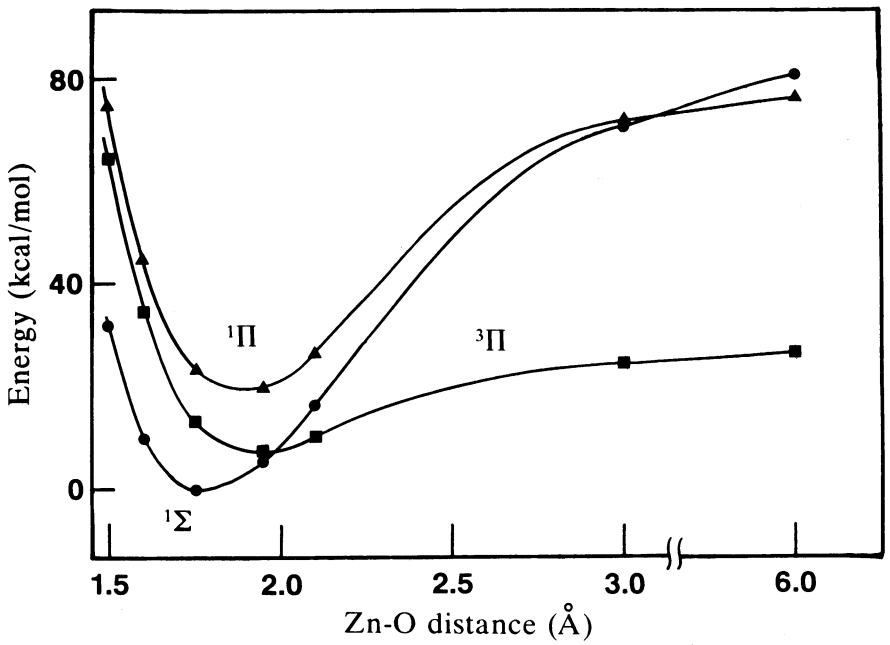

Figure 2. Potential energy curves of the lower singlet and triplet states of ZnO calculated by the SAC/SAC-CI method.

retical studies. They gave R_{eq} = 1.809 Å, D_e (dissociation energy) = 9.22 kcal/mol [7], and R_{eq} = 1.742 Å, D_e = 13.8 kcal/mol [5], though the experimental studies gave D_e = 65 ± 5 kcal/mol [19]. We calculate the ZnO molecule with the Madelung potential in order to see the influence of the outer field. The ZnO distance is fixed at the value of the crystal, 1.95 Å. Table I shows the dipole moments of the ground and excited states and the energy gap between the ground

TABLE I. Dipole moments (Debye) and the energy gaps (kcal/mol) between the $^1\Sigma^+$ ground state and the $^{1,3}\Pi$ excited states with and without the Madelung potential.

	Without Madelung potential					With Madelung potential	
	R = 1.76 Å		R = 1.95 Å			R = 1.95 Å	
State	μ	ΔE	μ	ΔE		μ	ΔE
$^1\Sigma^+$	−5.82	0	−6.18	0		−8.85	0
$^1\Pi$	−1.73	22.9	−2.52	14.5	A'	−4.12	39.7
					A''	−4.07	46.3
$^3\Pi$	−1.58	12.9	−2.06	1.8	A'	−5.34	51.3
					A''	−4.14	36.0

and excited states. The $^1\Sigma^+$ ground state is an ionic state with the polarization Zn^+O^- and the Madelung potential enhances the polarization from μ = 6.18 Debye to μ = 8.85 Debye. The energy gap between the $^1\Sigma^+$ and $^3\Pi$ states increases from 1.8 kcal/mol without the Madelung potential to 36.0 kcal/mol. The reason is that the Π state is an electron-transferred state from O to Zn against the Madelung potential and therefore is more unstable than in the free molecule.

B. ZnO + H_2 without Madelung Potential System

We examine the reaction path for the ZnO + H_2 without the Madelung potential system. The Zn—O distance is fixed at 1.95 Å. Figure 3 is a display of the reaction path calculated by the Hartree–Fock method and the forces acting on the H atoms. Figure 4 shows the potential energy diagram for the ground and excited states of this system calculated by the SAC/SAC–CI method. The geometry of the each point is shown in Table II. Ha is the proton on the left-hand side, and Hb, on the other side. At the initial points 1 and 2, the H—H distance is fixed at the length of a free H_2 molecule. Points 3, 4, 5, and 6 are located successively from the force vectors acting on the H atoms at the points 2, 3, 4, and 5, respectively. Point 7 is the most stable geometry from both the Hartree–Fock and the SAC method. The transition state of the reaction exists between points 3 and 4, as

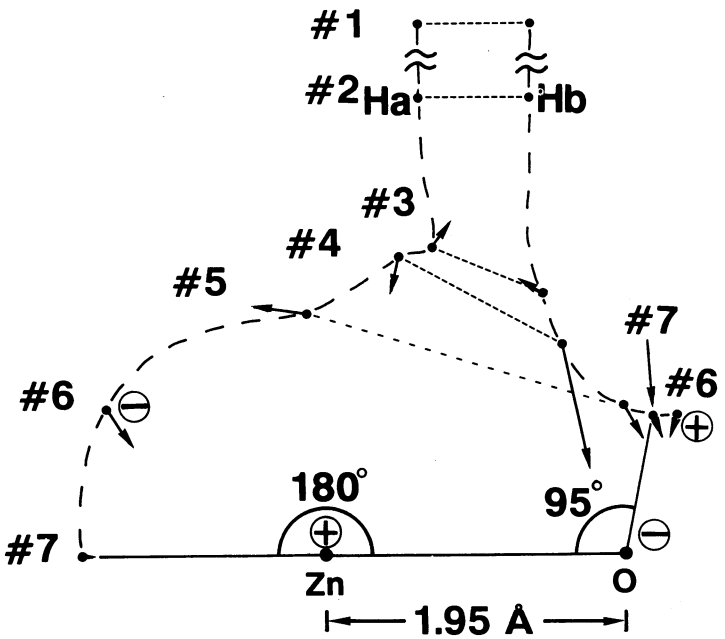

Figure 3. Forces acting on the H atoms in the ZnO + H_2 system along the reaction path shown in Table II.

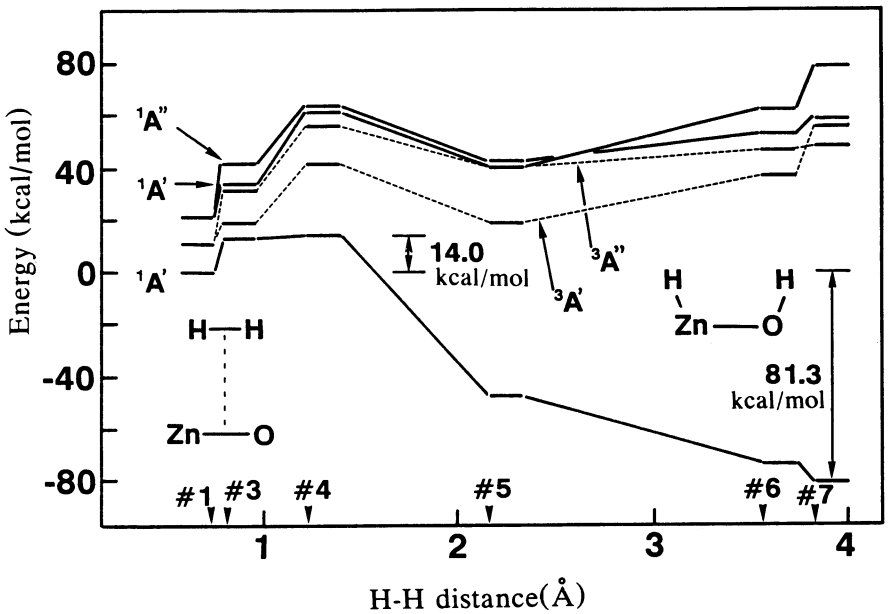

Figure 4. Potential energy diagram of the ground and several singlet and triplet excited states of the ZnO + H_2 system calculated by the SAC/SAC-CI method.

TABLE II. Geometries of points 1–7 along the reaction path of the ZnO + H_2 system shown in Figure 3.

Point	R_{H-H} (Å)	Ha		Hb	
		R_{H-Zn} (Å)	R_{H-O} (Å)	R_{H-Zn} (Å)	R_{H-O} (Å)
1	0.7417	10.0182	10.0902	10.0902	10.0182
2	0.7417	3.0602	3.2881	3.0602	3.2881
3	0.7846	1.7792	2.2795	2.3585	2.1190
4	1.2191	1.4320	2.0720	2.4450	2.0070
5	2.1674	0.9755	2.1846	2.6145	1.5992
6	3.7303	0.9675	2.4998	3.5062	1.7126
7	3.8397	0.9709	2.3297	3.5440	1.5940

seen in Figure 4. The H—Zn—O angle at point 7 is 180°, which is impossible on the surface, since the hydrogen conflicts with the neighboring O on the surface.

In Figure 4, the $^1A'$ state is the ground state and originates from the $^1\Sigma^+$ state of ZnO and the $^1\Sigma^+$ state of H_2, both being the ground states of the separated systems. It gives an exothermic potential curve with the heat of reaction of 81.3 kcal/mol and the reaction barrier of 14.0 kcal/mol. Other low-lying excited states give repulsive potential curves.

C. *Two-point Charges plus H_2 System*

To estimate the effect of the charges of ZnO on H_2, we replace Zn^+O^- by the two point charges (±0.5) placed at the positions of Zn and O and let H_2 approach along the reaction path shown in Figure 3. The energy is calculated by the full-CI method. We study the role of the electrostatic polarization of ZnO at the initial stage of the reaction. The energies of H_2 along the reaction path and the atomic charges on H are given in Table III. We see that the electrostatic potential works to stabilize the system before reaching the barrier. The electrostatic polarization at the place of ZnO induces a polarization of the σ_g MO of H_2 on the side of Ha, and the σ_u MO, on the other side. This effect increases the overlaps between the σ_g orbital of H_2 and the LUMO of ZnO and between the σ_u orbital of H_2 and the $2p\pi$ orbital of O. Therefore, the electrostatic potential makes the cleavage of H_2 easier.

D. *ZnO + H_2 system with Madelung Potential*

We finally study the ZnO + H_2 system with inclusion of the Madelung potential. The reaction path is the same as the one shown in Figure 3. Figure 5 is a display of the forces acting on the H atoms along the reaction path calculated by the Hartree–Fock method. Point 6 is the equilibrium geometry calculated by the Hartree–Fock method. At this point, the H—H distance is 3.73 Å, which is five times as large as the one of a free H_2. The H—H bond is completely broken. There the H—Zn—O angle is 146°, which is different from the angle 180° obtained without the Madelung potential. The H—O—Zn angle, on the other hand, is 111°, which is slightly larger than the 95° obtained without the Madelung potential. The reason is the electrostatic repulsion between the adsorbed hydrogen and the surrounding Madelung potential.

The potential energies along the path calculated by the SAC/SAC-CI method are shown in Figure 6. The energies of the ground and excited states do not change much from the one shown in Figure 4. Again, only the ground state is exothermic and the excited states are all repulsive. The heat of reaction is 73.5 kcal/mol

TABLE III. Energies and atomic charges of H_2 along the reaction path in which ZnO is replaced by the two point charges of ±0.5.

		With point charges		Without point charges
Point	R_{H-H} (Å)	ΔE (kcal/mol)	Atomic charge Ha/Hb	ΔE (kcal/mol)
2	0.7417	−0.19	−0.03/+0.03	0
3	0.7846	−10.23	0.00/0.00	0.69
4	1.2191	18.14	−0.05/+0.05	39.91
5	2.1674	43.36	−0.45/+0.45	97.70

The energy of H_2 at the equilibrium bond length and without the point charges is taken as a standard.

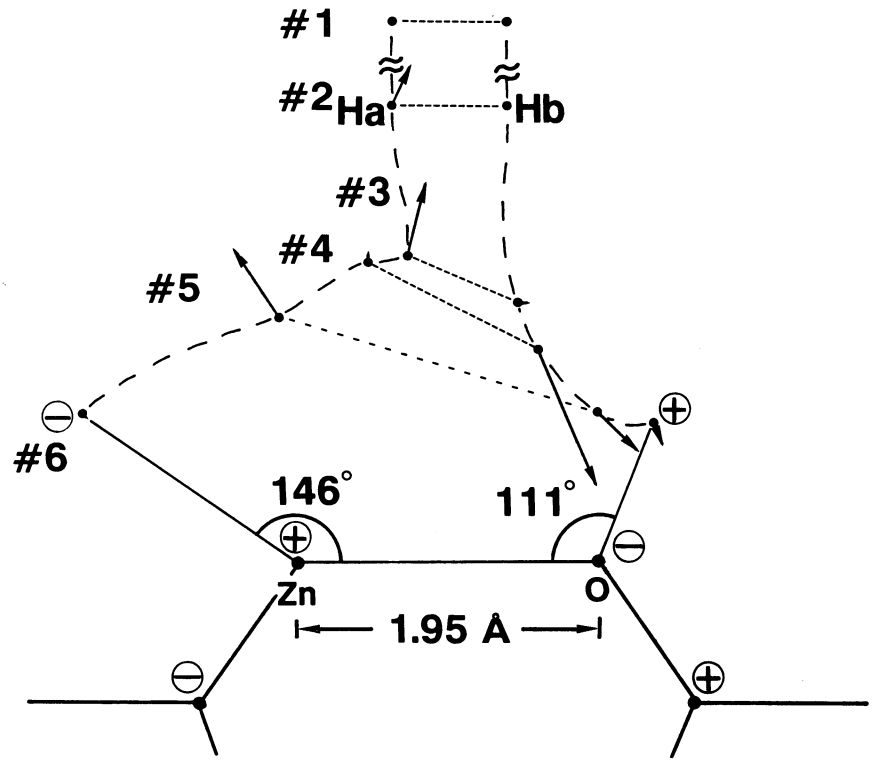

Figure 5. Forces acting on the H atoms in the ZnO + H_2 system with the Madelung potential along the reaction path shown in Figure 3.

and the reaction barrier is 11.5 kcal/mol. The Madelung potential lowers the barrier by 2.5 kcal/mol. The calculated vibrational frequencies ν_{O-H} and ν_{Zn-H} at point 6 are 4090 and 1730 cm^{-1} and are similar to the experimental values of 3510 and 1710 cm^{-1}, respectively.

Figure 7 shows the contour maps of the density difference defined by $\Delta\rho = \rho(ZnO{-}H_2) - \rho(ZnO) - \rho(H) - \rho(H)$. At point 2, the density of H_2 is polarized by the long-range electrostatic dipole field of Zn^+O^- with the right-hand-side hydrogen becoming protonic. There is a large difference between the densities at 3 and 4, though there is only a little difference in geometry between 3 and 4. It indicates that the transition state exists between 3 and 4 in accordance with the potential diagram given by Figure 4. At 5, the H—H bond is completely broken and the Zn—H and O—H bonds are formed. Along the Zn—H bond, the density in the left region of the Zn—H bond increases and induces to the left a force acting on the hydrogen. Then, the hydrogen moves, and at 6, the final Zn—H and O—H bonds are observed. Throughout the reaction, the density in the ZnO region does not decrease, indicating that the Zn—O bond is kept stable. This is related to the stability of the catalytic surface.

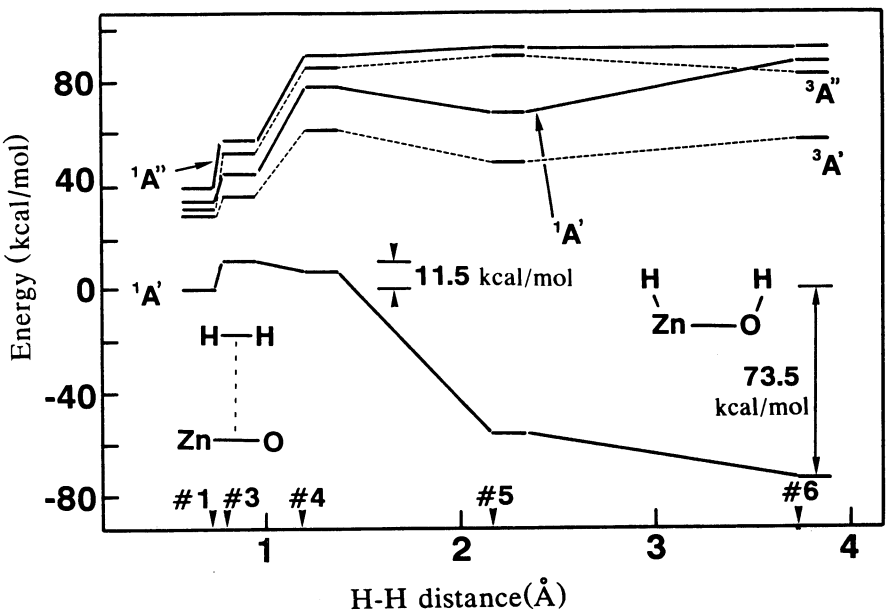

Figure 6. Potential energy diagram of the ground and several singlet and triplet excited states of the ZnO + H_2 system with the Madelung potential calculated by the SAC/SAC-CI method.

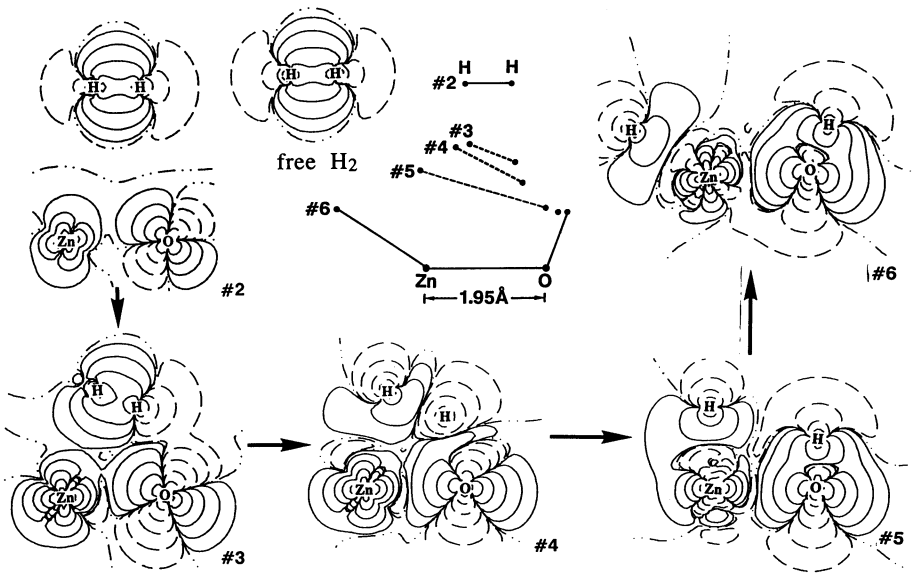

Figure 7. Reorganization of the electron density of the ZnO + H_2 system along the reaction path shown in Figure 3. The density difference is defined in the text.

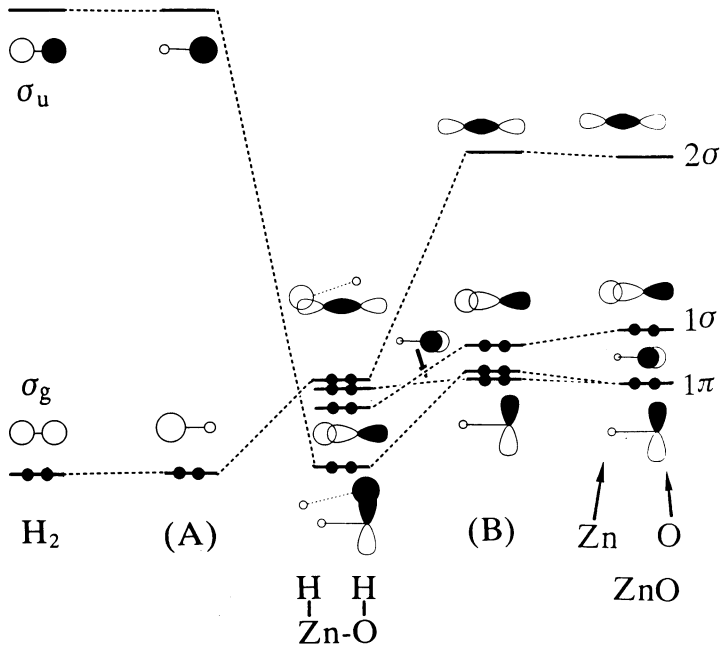

Figure 8. Orbital correlation diagram of the ZnO + H_2 system. (A) H_2 with the electrostatic field due to the poralization of Zn^+O^- at the point 3 of the H_2 + two point charges system; (B) ZnO with the Madelung potential.

The mechanism of this reaction is qualitatively explained by the orbital correlation diagram shown in Figure 8. The electron donation from the $2p\pi$ orbital of O to the antibonding σ_u MO of H_2 and the back-donation from the bonding σ_g MO of H_2 to the LUMO of ZnO are important. In the intermediate stage of the reaction, the charge polarization of ZnO works to increase the overlaps between these active MOS and makes the reaction easier. Throughout the reaction, another type of $2p\pi$ orbital of O, which is parallel to the surface, and the bonding HOMO of ZnO are inactive and work to keep the ZnO bond stable during the catalytic processes.

4. Conclusion

The ZnO molecule in the ground state both with and without the Madelung potential reacts with H_2 and dissociatively adsorbs it, making Zn—H and O—H bonds. Without the Madelung potential, the heat of reaction is 81.3 kcal/mol and the reaction barrier is 14.0 kcal/mol. With the Madelung potential, the heat of reaction is 73.5 kcal/mol and the barrier is 11.5 kcal/mol. The dissociative adsorption of H_2 on a ZnO surface studied here corresponds to the so-called type I adsorption. We note that we did not observe a molecularly adsorbed state. The calculated vibrational frequencies ν_{O-H} and ν_{Zn-H} at the dissociated geometry are 4090 and 1730 cm^{-1}, respectively, and are similar to the experimental values.

The mechanism of the dissociative adsorption of H_2 on a ZnO surface is the electron donation from the $2p\pi$ orbital of O to the antibonding σ_u MO of H_2 and the back-donation from the bonding σ_g MO of H_2 to the LUMO of ZnO. Throughout the reaction, the bonding σ orbital of ZnO is inactive and works to keep the ZnO bond stable during the catalytic processes.

The reactivity of the ZnO surface was analyzed and the following results were noted:

(a) The charge polarization in ZnO induces a polarization of the HOMO of H_2 on the side of O and LUMO on the other side, which makes the electron transfer and back-transfer interaction with ZnO easier, because such a deformation of MOS increases the overlaps between the active MOS of H_2 and ZnO.
(b) Among the lower-lying states of ZnO, only the $^1\Sigma^+$ state is catalytically active for the H_2 chemisorption. All the other low-lying states are repulsive. Although a free ZnO molecule has the $^2\Pi$ state in the vicinity of the $^1\Sigma^+$ state, the energy separation greatly increases in the ZnO cluster as an effect of the Madelung potential. The reason is that the $^3\Pi$ state is an electron-transferred state from O to Zn against the surrounding electrostatic field and therefore is more unstable than in the free ZnO molecule.
(c) The Madelung potential enhances the polarization of ZnO, namely, Zn^+O^-, and the reactivity with H_2 as a result. It also affects the geometry of the dissociatively adsorbed H_2 on a ZnO surface.

Acknowledgments

The calculations have been carried out with the FACOM M/780 computer at the Data Processing Center of Kyoto University and the HITAC M-680H at the Institute for Molecular Science. The authors thank the IMS computer center for the grants of computing time. Part of this study has been supported by a Grant-in-Aid for Scientific Research from the Japanese Ministry of Education, Science and Culture and by the Kurata Foundation.

Appendix

We show here a simple mathematical form of the electrostatic potential due to an array of charges on a surface. Though Evalt, Kornfeld, and others have shown the method of calculating the Madelung potential [20–22], they are for the inner region of a solid and are too complicated for the present purpose.

We consider a y–z plane in which positive and negative point charges are situated alternatively, as shown in Figure 1. Let ϕ be the scalar potential. In the region above the plane, the Poisson equation is

$$\Delta\phi = 0, \tag{A.1}$$

since there is no charge distribution. Considering the translational symmetry of the plane:

$$\phi(x, y, z) = \phi(x, y + nB, z) \tag{A.2}$$

$$= \phi(x, y, z + mA), \tag{A.3}$$

where A and B are the lattice constants along the z and y axes, respectively, shown in Figure 1 and n and m are integers. The charges are symmetrically located for the z–x plane and antisymmetrically located for the x–y plane:

$$\phi(x, y, z) = \phi(x, -y, z) \tag{A.4}$$

$$= -\phi(x, y, -z). \tag{A.5}$$

Any periodic value is represented by the summation of the sine waves by the Fourier's theorem. We suppose a function that satisfies Eqs. (A.2)–(A.5):

$$\phi(x, y, z) = \sum_{n=1, m=0} F_{n,m}(x) \sin(k_a n z) \cos(k_b m y), \tag{A.6}$$

where $k_a = 2\pi/A, k_b = 2\pi/B$. The terms with $n = 0$ do not satisfy Eq. (A.5), so they should be excluded.

It is easy to show the mathematical form of $F_{n,m}(x)$. Substituting Eq. (A.6) into Eq. (A.1), and operating Δ on ϕ term by term, we see that Eq. (A.1) holds only when

$$\left(\frac{\partial^2}{\partial x^2} + \frac{\partial^2}{\partial y^2} + \frac{\partial^2}{\partial z^2}\right) F_{n,m}(x) \sin(k_a n z) \cos(k_b m y)$$

$$= \frac{d^2}{dx^2} F_{n,m}(x) \sin(k_a n z) \cos(k_b m y)$$

$$- ((k_a n)^2 + (k_b m)^2) F_{n,m}(x) \sin(k_a n z) \cos(k_b m y) = 0. \tag{A.7}$$

Thus,

$$F_{n,m}(x) = C_{n,m} \exp(\pm\sqrt{(k_a n)^2 + (k_b m)^2}|x|) \sin(k_a n z) \cos(k_b m y), \tag{A.8}$$

where $C_{n,m}$ is a constant. The potential should vanish at $\pm\infty$; then, the sign of Eq. (A.8) must be minus:

$$F_{n,m}(x) = C_{n,m} \exp(-\sqrt{(k_a n)^2 + (k_b m)^2}|x|) \sin(k_a n z) \cos(k_b m y). \tag{A.9}$$

We need a boundary condition for determining the constant $C_{n,m}$. If x is large enough, ϕ would be nearly proportional to $\sin(k_a z)$ for fixed x and $\partial\phi/\partial y \sim 0$. So we suppose a boundary condition for a large enough fixed x_0 as

$$\phi(x_0, y, z) = C' \sin(k_a z). \tag{A.10}$$

The solution of Eq. (A.1) that satisfies Eq. (A.10) is

$$\phi(x, y, z) = C \exp(-k_a x) \sin(k_a z). \tag{A.11}$$

Equation (A.11) suggests that the electrostatic potential due to the ionic layer decreases exponentially. The third and fourth layers give 10.5% of the total electrostatic potential at the surface, and fifth and sixth layers give only 0.6%, so the effect of deeper layer than the second one may be neglected. We take into account the charges situated in the first and second layers alone.

We next consider the electric potential along the z axis. We consider a linear array that is made by the positive and negative point charges alternatively situ-

ated on the z axis as shown in Figure 1. $\Delta\phi = 0$ is supposed as the previous discussion. Using the cylindrical symmetry around the z axis, $\Delta\phi = 0$ is read as

$$\left(\frac{\partial^2}{\partial r^2} + \frac{1}{r}\frac{\partial}{\partial r} + \frac{\partial^2}{\partial z^2}\right)\phi(r,z) = 0, \tag{A.12}$$

where r is a radius from the z axis. Considering the translational symmetry of the plane:

$$\phi(r,z) = \phi(r,z + nA), \tag{A.13}$$

where A is the lattice constant along z axes shown in Figure 1 and n is integer. The charges are antisymmetrically located:

$$\phi(r,z) = -\phi(r,-z). \tag{A.14}$$

We suppose the function

$$\phi(r,z) = \sum_{n=1} F_n(r) \sin\left(\frac{2\pi nz}{A}\right) \tag{A.15}$$

as the one that satisfies Eqs. (A.13) and (A.14). The term with $n = 0$ does not satisfy Eq. (A.14) and so should be excluded.

Substituting Eq. (A.15) into Eq. (A.12), and operating Δ on ϕ term by term, we see that Eq. (A.12) holds only when

$$\left(\frac{\partial^2}{\partial r^2} + \frac{1}{r}\frac{\partial}{\partial r} + \frac{\partial^2}{\partial z^2}\right) F_n(r) \sin(knz)$$
$$= \frac{d^2}{dr^2}F_n(r) \sin(knz) + \frac{1}{r}\frac{d}{dr}F_n(r) \sin(knz) - (kn)^2 Fn(r) \sin(knz) = 0, \tag{A.16}$$

where $k = 2\pi/A$. Thus,

$$F_n(r) = \frac{C_n}{\sqrt{r}} \exp(-knr)\left(1 - \frac{1}{4(knr)^2} + \frac{1}{(knr)^3} - \ldots\right), \tag{A.17}$$

where C_n is a constant. We need a boundary condition for determining the constant C_n. If r is large enough, ϕ would be nearly proportional to $\sin(kz)$ for fixed r. So we suppose a boundary condition for a large enough r_0 as

$$\phi(r_0,z) = C' \sin(kz). \tag{A.18}$$

The solution of Eq. (A.12) is

$$\phi(r,z) = \frac{C}{\sqrt{r}} \cos(kz) \exp(-kr)\left(1 - \frac{1}{4(kr)^2} + \frac{1}{(kr)^3} - \ldots\right). \tag{A.19}$$

If $r > A$, the first term of this expansion is dominant. So,

$$\phi(r,z) = \frac{C}{\sqrt{r}} \cos(kz) \exp(-kr) \tag{A.20}$$

approximates the electrostatic potential. Equation (A.20) suggests that the electrostatic potential decreases more rapidly than does the exponential. The second-neighbor array shown in Figure 1 gives 7.4% of the total electrostatic potential at the position of ZnO interacting with H_2, and the third-neighbor array gives 0.8%, the fourth-neighbor array gives 0.1%, and so on. Therefore, we take into account the charges situated only in the first-, second-, and third-neighbor linear array.

Bibliography

[1] A. L. Dent and R. J. Kokes, J. Phys. Chem. **73**, 3781 (1969).
[2] W. C. Conner, Jr. and R. J. Kokes, J. Catal. **36**, 199 (1975).
[3] A. B. Anderson and J. A. Nichols, J. Am. Chem. Soc. **108**, 4742 (1986).
[4] C.W. Bauschlicher, Jr. and S. R. Langhoff, Chem. Phys. Lett. **126**, 163 (1986).
[5] M. Dolg, U. Wedig, and H. Preuss, J. Chem. Phys. **86**, 2123 (1987).
[6] O. Gropen, U. Wahlgren, and L. Pettersson, Chem. Phys. **66**, 459 (1982).
[7] M. Witko and V. B. Koutecky, Int. J. Quantum Chem. **24**, 1535 (1986).
[8] P. J. Hay and W. R. Wadt, J. Chem. Phys. **82**, 270 (1985).
[9] (a) S. Huzinaga, J. Chem. Phys. **42**, 1293 (1965); (b) T. H. Dunning, Jr. *Ibid.* **53**, 2823 (1970).
[10] (a) H. Nakatsuji, K. Kanda, and T. Yonezawa, Chem. Phys. Lett. **75**, 340 (1980); (b) H. Nakatsuji, T. Hayakawa, and M. Hada, *Ibid.* **80**, 94 (1981).
[11] H. Nakatsuji and K. Hirao, J. Chem. Phys. **68**, 2053 (1978).
[12] H. Nakatsuji, Chem. Phys. Lett. **59**, 362 (1978); *Ibid.* **67**, 329, 334 (1979).
[13] H. Nakatsuji, Chem. Phys. **75**, 425 (1983).
[14] B. R. Brooks, P. Saxe, W. D. Laidig, and M. Dupuis, Program Library No. 481 (Computer Center of the Institute for Molecular Science, Okazaki, 1981).
[15] H. Nakatsuji, Program Library No. 146 (Y4/SAC) (Data Processing Center of Kyoto University, 1985); Program Library SAC85, No. 1396 (Computer Center of the Institute for Molecular Science, Okazaki, 1981).
[16] G. Heiland, P. Kurstman, and H. Pfister, Z. Phys. **176**, 485 (1963).
[17] W. A. Harrison, Phys. Rev. B **10**, 767 (1974).
[18] J. C. Phillips, *Covalent Bonding in Crystals, Molecular and Polymers* (University of Chicago Press, Chicago, 1969).
[19] (a) B. G. Wicke, J. Chem. Phys. **78**, 6036 (1983); (b) D. F. Anthrop and A.W. Searcy, J. Phys. Chem. **68**, 2335 (1964).
[20] (a) P. P. Evald, Ann. Phys. **64**, 253 (1921); (b) H. Kornfeld, Z. Phys. **22**, 27 (1924).
[21] R.W. Nosker, P. Mark, and J. D. Levine, Surf. Sci. **19**, 291 (1970).
[22] R. E. Watson, M. L. Perlman, and J.W. Davenport, Surf. Sci. **115**, 117 (1982).

Received October 29, 1990
Accepted for publication April 18, 1991